iScience

CellPress
OPEN ACCESS

Article

Piezo1 induces endothelial responses to shear stress via soluble adenylyl Cyclase-IP_3R2 circuit

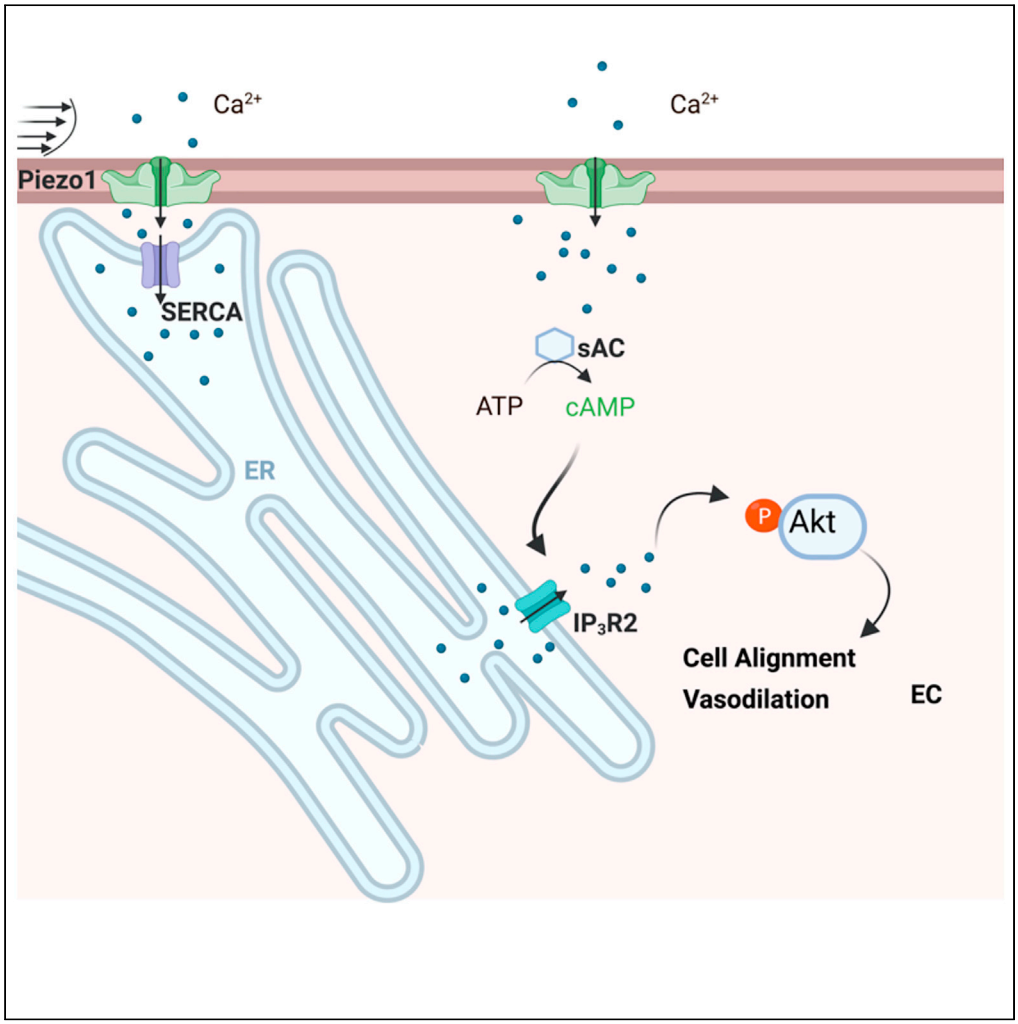

Dianicha Santana Nunez, Asrar B. Malik, Quinn Lee, ..., Irena Levitan, Dolly Mehta, Yulia A. Komarova

ykomarov@uic.edu

Highlights

Piezo1 activation leads to the rapid sequestration of Ca^{2+} into the ER lumen through SERCA

Piezo1 activation leads to Ca^{2+} release from cAMP sensitive IP_3R2 stores

ER Ca^{2+} release induces Akt activity and EC alignment in response to shear stresses

Piezo1-mediated Akt activity induces vasodilation in response to increased flow

Santana Nunez et al., iScience 26, 106661
May 19, 2023
https://doi.org/10.1016/j.isci.2023.106661

iScience

CellPress
OPEN ACCESS

Article

Piezo1 induces endothelial responses to shear stress via soluble adenylyl Cyclase-IP_3R2 circuit

Dianicha Santana Nunez,[1] Asrar B. Malik,[1] Quinn Lee,[1] Sang Joon Ahn,[2] Arnold Coctecon-Murillo,[1] Dana Lazarko,[2] Irena Levitan,[2] Dolly Mehta,[1] and Yulia A. Komarova[1,3,*]

SUMMARY

Endothelial cells (ECs) continuously sense and adapt to changes in shear stress generated by blood flow. Here, we show that the activation of the mechanosensitive channel Piezo1 by defined shear forces induces Ca^{2+} entry into the endoplasmic reticulum (ER) via the ER Ca^{2+} ATPase pump. This entry is followed by inositol trisphosphate receptor 2 (IP_3R2)-elicited ER Ca^{2+} release into the cytosol. The mechanism of ER Ca^{2+} release involves the generation of cAMP by soluble adenylyl cyclase (sAC), leading to IP_3R2-evoked Ca^{2+} gating. Depleting sAC or IP_3R2 prevents ER Ca^{2+} release and blocks EC alignment in the direction of flow. Overexpression of constitutively active Akt1 restores the shear-induced alignment of ECs lacking Piezo1 or IP_3R2, as well as the flow-induced vasodilation in endothelial restricted Piezo1 knockout mice. These studies describe an unknown Piezo1-cAMP-IP_3R2 circuit as an essential mechanism activating Akt signaling and inducing adaptive changes in ECs to laminar flow.

INTRODUCTION

Endothelial cells (ECs) lining the vessel intima are continuously exposed to recurring alterations in local fluid shear stress,[1,2] variations in hydrostatic pressure in the capillaries,[3,4] and changes in vessel wall tensile strain during increased vascular pulsations.[5] These localized changes in mechanical forces, such as fluid shear stress, are integral to normal perfusion. Fluid shear stress, the frictional force generated by distinct spatial and temporal blood flow patterns, is the most relevant factor in developmental and physiological vascular processes.[1,6,7] These processes include angiogenesis,[6] as well as the maintenance of blood pressure and flow patterns[1,2,7] needed to ensure normal blood perfusion in vital organs such as the brain and heart.[8–10]

It is now apparent that ECs sense forces such as shear stress by engaging multiple mechanosensitive proteins, including G-protein-coupled receptors,[11,12] adherens junction proteins,[13,14] and flow-sensitive ion channels including the recently discovered Piezo-type mechanosensitive ion channel component 1 (Piezo1).[15–17] Piezo1 is a well-established mechanosensitive channel, which non-selectively transports Ca^{2+} from the extracellular milieu to the cytosol of ECs in response to mechanical forces.[18–20] Deleting the *Piezo1* gene in mice reduces the level of shear-evoked increases in intracellular Ca^{2+}[18] as well as prevents the morphological and cytoprotective responses of ECs to shear force.[18,21] Impairment or loss of Piezo1 activity severely compromises vascular development and angiogenesis[18,19] and induces hypertension in adult mice.[22] However, signaling mechanisms that control EC adaptation to shear stress downstream of Piezo1 remain poorly understood.

Shear stress induces both Ca^{2+} entry from the extracellular milieu through mechanosensitive channels, and Ca^{2+} release from inositol 1,4,5-trisphosphate receptors (IP3Rs) localized in the ER membrane.[23] A fundamental question is whether these two mechanotransduction pathways are intrinsically linked for regulating EC adaptation to sheer stress. Piezo1 channel, which interacts with and modulates the activity of the sarco/endoplasmic reticulum Ca^{2+} ATPase (SERCA) pump,[24] may activate both Ca^{2+} entry from the extracellular milieu and Ca^{2+} release from the ER stores. Here, the data show that the activation of Piezo1 by shear stress leads to the rapid mobilization of intracellular Ca^{2+} into the ER lumen followed by ER Ca^{2+} release via a sAC-cAMP sensitive mechanism. In contrast to previous studies showing phospholipase C (PLC)-mediated Ca^{2+} release from the ER stores via an IP_3-IP_3R cascade,[25,26] the data, described here, link Piezo1 mechanosensing to a cAMP-dependent ER Ca^{2+} release through IP_3R2. This Piezo1-sAC-IP_3R2

[1]Department of Pharmacology and Regenerative Medicine, the Center for Lung and Vascular Biology, University of Illinois College of Medicine, Chicago, IL, USA

[2]Department of Medicine, University of Illinois College of Medicine, Chicago, IL, USA

[3]Lead contact

*Correspondence: ykomarov@uic.edu

https://doi.org/10.1016/j.isci.2023.106661

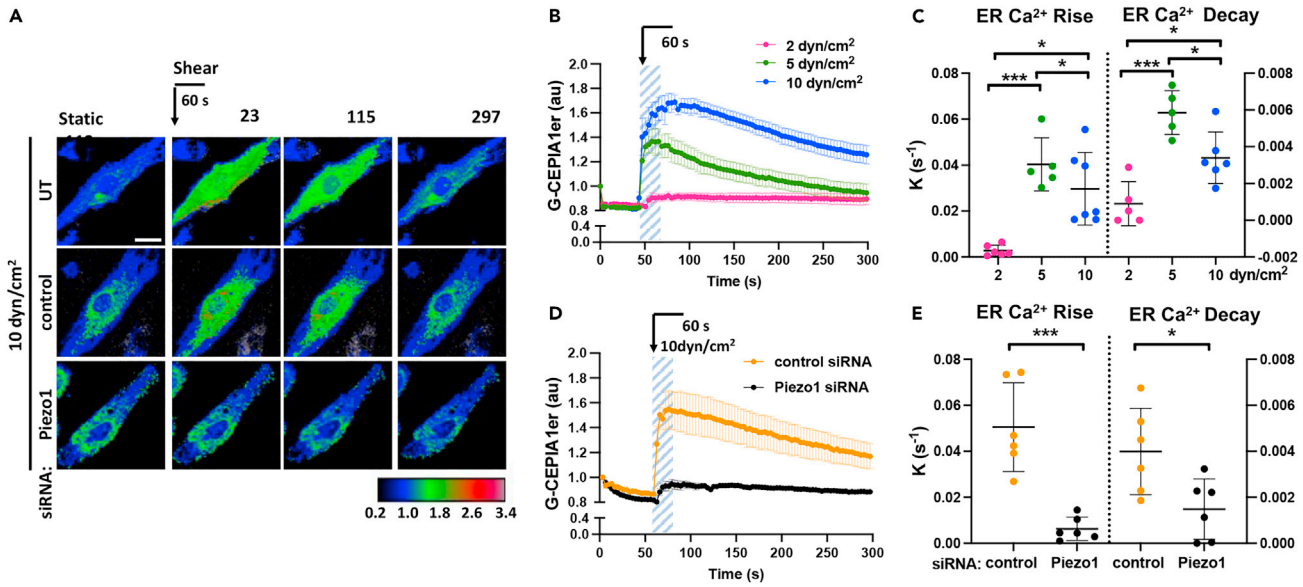

Figure 1. Shear stress activation of Piezo1 induces rapid mobilization of Ca^{2+} into the ER lumen

(A) Live-cell images of G-CEPIA1er, used to measure changes in $[Ca^{2+}]_{ER}$, upon the application of 10 dyn/cm^2 laminar shear for 60 s in untransfected (UT) or siRNA-treated endothelial monolayers as indicated; color-coding scale is shown below; times in seconds; scale bar, 20 μm. Arrow indicates the application of shear stress.

(B) Time-dependent changes of $[Ca^{2+}]_{ER}$ in endothelial monolayers before and after stimulation with 2, 5, and 10 dyn/cm^2 shear stress for 60 s (highlighted area) as in (A); n = 5-7 cells per group from 3 independent experiments; mean ± SEM.

(C) Rate constants of ER Ca^{2+} rise and decay in (B), mean ± SD; *, $p < 0.05$; ***, $p < 0.001$, ANOVA with Tukey's post hoc test.

(D) Time-dependent changes of $[Ca^{2+}]_{ER}$ in control and Piezo1-depleted endothelial monolayers upon the application of 10 dyn/cm^2 shear stress as in (A); n = 6 cells per group from 3 independent experiments; mean ± SEM.

(E) Rate constants of ER Ca^{2+} rise and decay in D, mean ± SD; left, *, $p < 0.05$; ***, $p < 0.001$, Student's *t* test.

mechanotransduction circuit plays a critical role in the activation of Akt signaling as a part of the adaptive morphological response of ECs to laminar shear stress causing vessel vasodilation.

RESULTS

Shear stress activation of Piezo1 in endothelial cells induces rapid mobilization of intracellular Ca^{2+} into the endoplasmic reticulum lumen

To determine the role of Piezo1 in shear stress-induced ER Ca^{2+} signaling, we exposed endothelial monolayers to laminar fluid shear forces of 5 and 10 dyn/cm^2, stresses known to stimulate adaptive morphological response in ECs.[1] We also exposed endothelial cell monolayers to lower level laminar flow of 2 dyn/cm^2, as it does not induce EC adaptive morphological changes.[1] The temporal changes in $[Ca^{2+}]_{ER}$ were measured using the ER-targeted Ca^{2+} sensor G-CEPIA1er, which emits fluorescence when bound to ER Ca^{2+}.[27] Exposure of human pulmonary arterial endothelial (HPAE) monolayers to 5 and 10 dyn/cm^2 shear forces for 60s increased fluorescence in the ER, indicative of increased $[Ca^{2+}]_{ER}$ (Figures 1A and 1B). These changes were dependent on the shear forces applied and were far less apparent in cells exposed to 2 dyn/cm^2 shear (Figures 1A and 1B). Furthermore, the amplitude of $[Ca^{2+}]_{ER}$ increased proportionally to the shear force applied (Figures S1A and S1B), whereas the rate constants calculated for ER Ca^{2+} rise and decay were lower at higher shear force (Figure 1C). Similar kinetics were also observed in human aortic endothelial (HAE) monolayers subjected to 10 dyn/cm^2 laminar shear stress (Figures S1C–S1F), indicating the generalizability of our finding to arterial ECs of different vascular beds.

Depletion of Piezo1 abrogated the transient increase in $[Ca^{2+}]_{ER}$, leading to the reduction of both rise and decay constants in ECs exposed to the stresses applied (Figures 1A, 1D, 1E, S1G, and S1H). Consistent with previous reports,[18] depletion of Piezo1 also markedly diminished the cytosolic Ca^{2+} rise in response to shear stress (Figures S1I and S1J). Thus, these results revealed the central role of Piezo1 in regulating Ca^{2+} homeostasis via a rapid mobilization of Ca^{2+} into the ER in response to shear stresses applied.

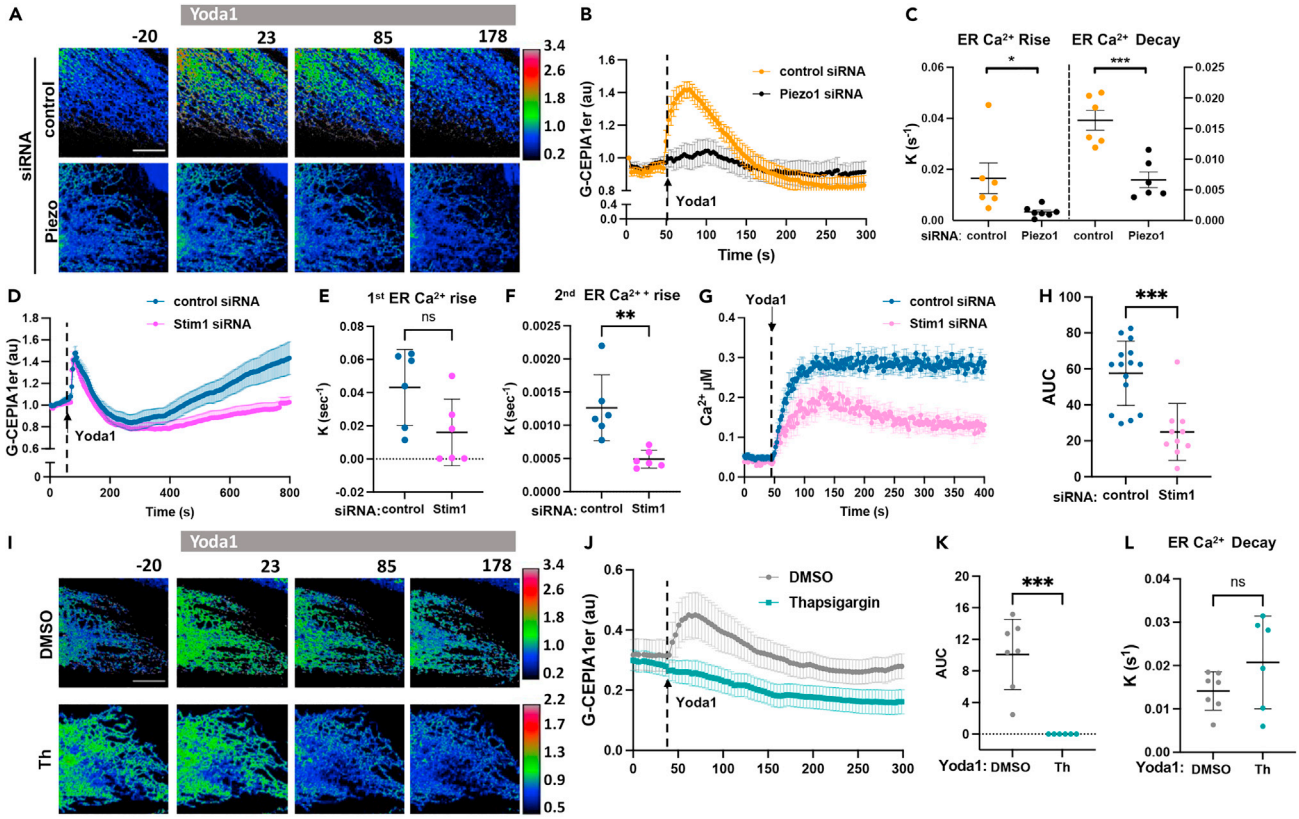

Figure 2. Activation of Piezo1 with Yoda induces SERCA-dependent uptake of Ca^{2+} in the ER lumen

(A) Live-cell images of G-CEPIA1er in endothelial monolayers pre-treated with control or Piezo1 siRNA and stimulated with the Piezo1 activator Yoda1 at time 0; color-coding as in Figure 1A; time in seconds; scale bar, 10 µm.

(B) Time-dependent changes of $[Ca^{2+}]_{ER}$ upon Piezo1 activation using Yoda1 in (A); n = 6 cells per group from 3 independent experiments; mean ± SEM.

(C) Rate constants of ER Ca^{2+} rise and decay calculated from data in (B); mean ± SD; *, $p < 0.05$, Student's *t* test; ***, $p < 0.001$, Student's *t* test.

(D) Time course of $[Ca^{2+}]_{ER}$ in endothelial monolayers pre-treated with control or STIM1 siRNA and stimulated with Yoda1 (arrow); n = 6 cells per group from 2 independent experiments; mean ± SEM.

(E and F) Rate constants of the first (E) and the second (F) rise of ER Ca^{2+} calculated from data in (D), mean ± SD; ns, not significant, Student's *t* test; **, $p < 0.01$, Student's *t* test.

(G) Time-dependent changes of cytosolic $[Ca^{2+}]_i$ on the activation of Piezo1 with Yoda1 (arrow) in endothelial monolayers pre-treated with control or STIM1 siRNA; n = 10-17 cells per group from 2 independent experiments; mean ± SEM.

(H) Changes of $[Ca^{2+}]_i$ within the first 350s (area under the curve) after Yoda1 stimulation calculated from data in (F); mean ± SD; ns, not significant, Student's *t* test; ***, $p < 0.001$, Student's *t* test.

(I) Live-cell images of G-CEPIA1er before and after the activation of Piezo1 with Yoda1 in endothelial monolayers pre-treated with vehicle (DMSO) or thapsigargin (Th) to inhibit SERCA; color-coding as in Figure 1A; note, different scale ranges are used to demonstrate ER Ca^{2+} kinetics in cells inhibited of SERCA; time in seconds; scale bar, 10µm.

(J) Time-dependent changes of $[Ca^{2+}]_{ER}$ in (H); n = 6-7 cells per group from 3 independent experiments; mean ± SEM.

(K and L) Changes in ER Ca^{2+} (area under the curve) following Yoda1 treatment (K) and rate constants of ER Ca^{2+}decay (L) calculated from data in (J); mean ± SD; ***, $p < 0.001$, Student's *t* test.

Piezo1 cooperates with sarco/endoplasmic reticulum Ca^{2+} ATPase to induce the rapid mobilization of Ca^{2+} into the endoplasmic reticulum

We next addressed whether the activation of Piezo1 can induce changes in $[Ca^{2+}]_{ER}$ independent of mechanical stress. Here using Yoda1, a specific Piezo1 activator,[28] we also observed transient increases in $[Ca^{2+}]_{ER}$ (Figures 2A–2C). Similar to cells exposed to laminar flow, activation of Piezo1 with Yoda1 led to a rapid transient increase in ER Ca^{2+} (Figures 2A–2C). This response was prevented by Piezo1 knockdown, indicative of the specificity of Yoda1 in activating Piezo1 (Figures 2A–2C). Depletion of extracellular Ca^{2+} also abolished the rapid mobilization of Ca^{2+} into the ER (Figures S2A and S2B). Furthermore, the rate constants of ER Ca^{2+} rise and decay were significantly greater in Yoda1-stimulated ECs as compared to ECs treated with diacylglycerol (DAG) analogue 1-oleoyl-2-acetyl-*sn*-glycerol (OAG) (Figures S2C and S2D),

the activator of receptor-operated Ca^{2+} entry,[29] suggesting a different mechanism of Ca^{2+} mobilization into the ER induced by Piezo1 as compared to receptor-operated Ca^{2+} entry.

To investigate the role of STIM1, which translocates to the plasma membrane upon ER Ca^{2+} depletion to activate store-operated Ca^{2+} entry[30,31] in rapid mobilization of Ca^{2+} into the ER lumen upon the activation of Piezo1, we repeated these studies in STIM1 depleted cells (Figures 2D and 2E). Interestingly, STIM1 depletion (Figures S2E and S2F) did not affect the kinetics of rapid rise in the ER Ca^{2+} but decreased the rate constant of the second much slower rise in ER Ca^{2+} (Figures 2D–2F). Consistent with the role of STIM1 in activating store-operated Ca^{2+} entry, the depletion of STIM1 also altered the kinetics of Yoda1-induced increases in intracellular Ca^{2+} (Figures 2G and 2H). Whereas control ECs showed a sustained increase in intracellular Ca^{2+} upon challenge with Yoda1, cells depleted of STIM1 showed a transient increase in intracellular Ca^{2+} (Figures 2G and 2H). We concluded that STIM1 did not contribute to the rapid rise in ER Ca^{2+} following Piezo1 activation but was necessary to replenish the ER Ca^{2+} upon depletion.

We also addressed the role of the SERCA pump in regulating Piezo1-mediated ER Ca^{2+} entry. As Piezo1 and SERCA interact both *in vitro* and in cells,[24] Piezo1 function may be coupled to the activation of the SERCA pump. Thus, we inhibited SERCA using the specific non-competitive inhibitor thapsigargin,[32] and determined the role of SERCA in the Piezo1-induced mobilization of Ca^{2+} into the ER. We demonstrated that thapsigargin abrogated Yoda1-induced rise in the ER Ca^{2+} (Figures 2I–2K), but it had no significant effect on ER Ca^{2+} decay (Figures 2J and 2L), which occurred at the same rate as in DMSO-treated cells. ECs treated with thapsigargin showed a trend toward higher decay constants as the result of passive leakage of ER Ca^{2+}, which became more apparent when SERCA pump activity was inhibited. Thus, SERCA activity was required for Piezo1-mediated rise in ER Ca^{2+} but not ER Ca^{2+} decay.

Activation of Piezo1 induces Ca^{2+} release through IP_3R2

To address the mechanism of ER Ca^{2+} decay downstream of Piezo1, we depleted IP_3R2 and IP_3R3, two inositol trisphosphate receptors highly expressed on the ER membrane of ECs[33,34]. Depletion of IP_3R3 had no effect on Piezo1-induced ER Ca^{2+} decay since the rate constants were similar to control siRNA-treated cells (Figures 3A–3C and S3A–S3C). In contrast, the depletion of IP_3R2 significantly reduced the rate constant of ER Ca^{2+} decay without affecting the rate constant of ER Ca^{2+} rise (Figure 3A–3C, S3C, and S3D). Similarly, depletion of IP_3R2 significantly diminished the rate constant of ER Ca^{2+} decay upon the application of laminar shear stress (Figures 3D–3F).

Depletion of either receptor did not result in the compensatory upregulation of the other receptor (Figures S3A–S3D). Furthermore, in contrast to IP_3R3 depletion, which had no effect on Piezo1-mediated changes in intracellular $[Ca^{2+}]_i$ (Figures S3E and S3F), depletion of IP_3R2 significantly reduced increases in $[Ca^{2+}]_i$ following the activation of Piezo1 with Yoda1 or by applying laminar shear stresses (Figures S3G–S3J). These data suggest that the IP_3R2 pathway was essential for the release of ER Ca^{2+} into the cytosol following mechanical or pharmacological activation of Piezo1.

Piezo1 activation of soluble adenyl cyclase induces cAMP-dependent endoplasmic reticulum Ca^{2+} release

To investigate the signaling mechanism of Ca^{2+} release from the ER downstream of Piezo1, we studied the role of cAMP in sensitizing ER calcium release through IP_3R2 stores. The second messengers IP_3 and free intracellular Ca^{2+} activate all IP_3Rs,[33,35] whereas cAMP exclusively sensitizes IP_3R2.[36–38] Since Ca^{2+} directly stimulates soluble-adenylate cyclase (sAC),[39] we determined whether the influx of Ca^{2+} through Piezo1 activated sAC and induced the production of cAMP. We measured relative changes in cAMP concentrations using the cAMP sensor EPAC1, a guanine nucleotide exchange factor directly activated by cAMP, tagged to a circularly permuted GFP protein.[40] Yoda1 increased GFP intensity of the cAMP sensor in endothelial monolayers (Figure 4A), indicative of the increased generation of cAMP.

Furthermore, depletion of sAC significantly reduced Yoda1-induced production of cAMP (Figures 4A, 4B, S4A, and S4B), suggesting that sAC was crucial in mediating cAMP generation downstream of Piezo1 activation. Furthermore, depletion or pharmacological inhibition of sAC with bithionol markedly reduced the rate constant of ER Ca^{2+} decay (Figures 4C–4E and S4C–S4E) as well as delayed the increase in cytosolic $[Ca^{2+}]_i$ following pharmacological or shear-mediated activation of Piezo1 (Figures S4F–S4I). Thus, sAC

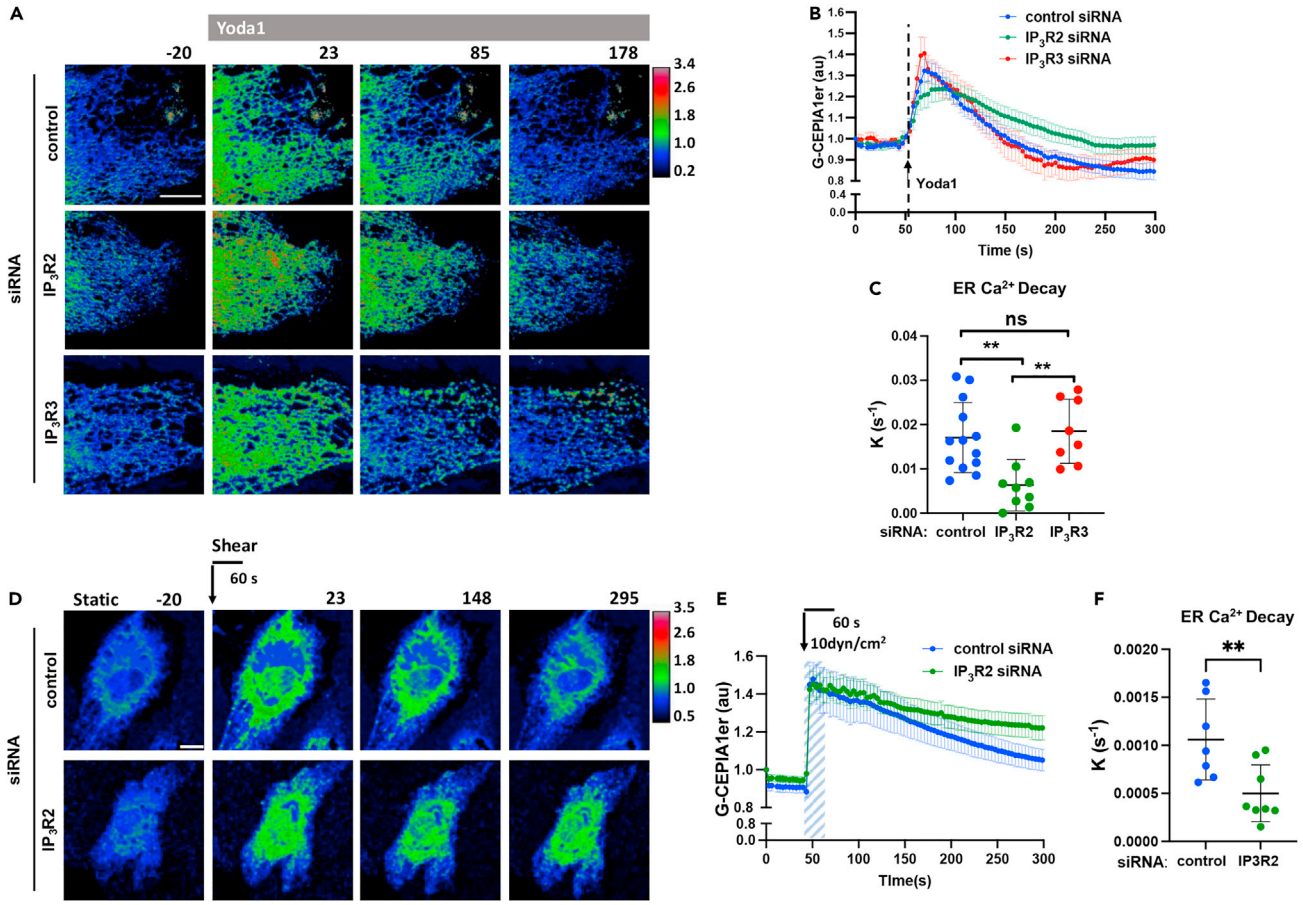

Figure 3. Activation of Piezo1 induces ER Ca^{2+} store release via IP_3R2 channel

(A) Live-cell images of G-CEPIA1er upon the activation of Piezo1 with Yoda1 of endothelial monolayers pre-treated with control, IP_3R2, or IP_3R3 siRNA; color-coding as in Figure 1A; time in seconds; scale bar, 10 μm.

(B) Time course of $[Ca^{2+}]_{ER}$ in (A); n = 8-12 cells per group from 3 independent experiments; mean ± SEM.

(C) Rate constants of ER Ca^{2+} decay calculated form data in (B); mean ± SD; **, $p < 0.01$; ANOVA with Tukey's post hoc test.

(D) Live-cell images of G-CEPIAer in control and IP_3R2 deficient endothelial monolayers upon the application of 10 dyn/cm^2 laminar shear for 60 s; time in seconds; scale bar, 10 μm.

(E) Time course of $[Ca^{2+}]_{ER}$ in (D); n = 7-9 cells per group from 3 independent experiments; mean ± SEM.

(F) Rate constants of ER Ca^{2+} decay calculated form data in (E); mean ± SD; **, $p < 0.01$, Student's *t* test.

activation was essential for Piezo1-induced generation of cAMP and Ca^{2+} release through cAMP-sensitized IP_3R2 stores.

Endoplasmic reticulum Ca^{2+} release through IP_3R2 channel is required for the Akt-dependent response of endothelial cells to shear stress

ECs lacking Piezo1 failed to induce Akt1 phosphorylation and became aligned in the direction of laminar flow.[18,19,22] Thus, we determined whether ER Ca^{2+} release as well as Akt1 activity were required for the adaptive reorientation of ECs as induced by flow. As compared to endothelial monolayers grown under static conditions, both HPAE and HAE monolayers subjected to 10 dyn/cm^2 shear stress for 24h had greater incidence of F-actin filaments with a smaller angle (0°-30°) relative to the direction of flow, indicative of cell alignment shift (Figures 5A, 5B and S5A–S5F). The alignment, however, was lost in cells depleted of either Piezo1 or IP_3R2, as apparent from a significant decrease in the incidence of filaments aligned to flow (0°-30°) and an increase in randomly distributed filaments (forming larger angles to flow) (Figures 5A, 5B and S5A–S5F). Similar to Piezo1 depletion,[22] IP_3R2 deficiency prevented shear-induced phosphorylation of Akt at S473 (Figures 5C and 5D), the site required for the maximal enzymatic activation of Akt.[41]

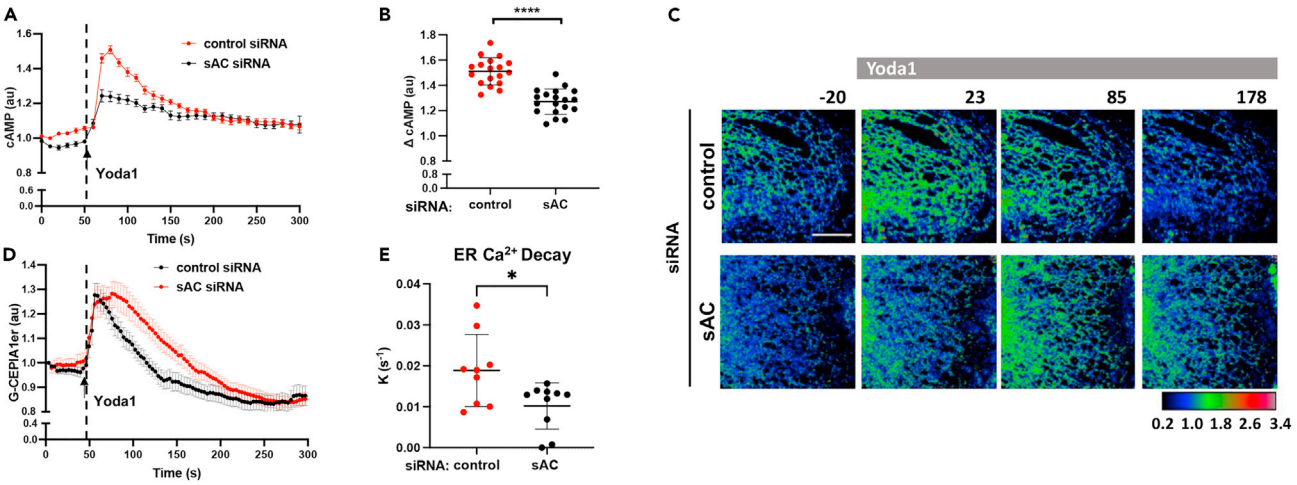

Figure 4. Activation of Piezo1 induces sAC-dependent generation of cAMP and cAMP-evoked ER Ca^{2+} release

(A) Time-dependent changes of cAMP concentrations upon the activation of Piezo1 with Yoda1 (arrow) in control and sAC-depleted endothelial monolayers; n = 18 cells per group from 3 independent experiments; mean ± SEM.

(B) Relative changes of cAMP concentrations in (A); mean ± SD; ****, $p < 0.0001$, Student's *t* test.

(C) Live-cell images of G-CEPIA1er upon the activation of Piezo1 with Yoda1 (arrow) in control and sAC-depleted endothelial monolayers; color-coding as in Figure 1A; times in seconds; scale bar, 10 μm.

(D) Time-dependent changes of $[Ca^{2+}]_{ER}$ in (C); n = 7-10 cells per group from 3 independent experiments; mean ± SEM.

(E) The rate constants of ER Ca^{2+} decay calculated from data in (C); mean ± SD; *, $p < 0.05$, Student's *t* test.

Since the depletion of Piezo1 or IP_3R2 prevented both shear-induced activation of Akt and alignment of ECs in the direction of flow, we next addressed the role of Akt kinase in mediating the adaptive morphological response to shear stresses. Expression of an activation-deficient Akt1 mutant[42] prevented the alignment of ECs in the direction of flow (Figures 6A, 6B, S5G, and S5H). We additionally determined whether ectopic expression of constitutively active (myr)-Akt1[42] would restore the response of ECs lacking Piezo1 or IP_3R2 to shear stress. We observed that myr-Akt1 restored the alignment of ECs depleted of either Piezo1 or IP_3R2 (Figures 6C, 6D, S5I, and S5J). However, this response was not seen in Piezo1-or IP_3R2-depleted cells expressing the empty vector (Figures 6C, 6D, S5I, and S5J). Thus, the loss of either Piezo1 or IP_3R2 each prevented the adaptive response of ECs to shear stress by limiting Akt signaling.

Furthermore, to address the physiological implication of Piezo1 in regulating the Akt-mediated response of ECs to laminar shear stress, we transduced either empty control vector or myr-Akt1 in ECs of mesenteric vessels isolated from endothelial-restricted knockout of *Piezo1* mice ($Piezo1^{\Delta EC}$), which showed markedly reduced vasodilation response to increased fluid shear as compared to control wild-type (WT) mice (Figures 6E and 6F). We observed that the expression of myr-Akt1, but not the control vector, restored the flow-induced vasodilation response of mesenteric vessels *ex vivo* to the level of control vessels (Figures 6E and 6F). These data cumulatively suggest that the Piezo1-sAC-IP_3R2 circuit is responsible for the activation of Akt1 signaling in ECs and thereby, the spatial and temporal response of blood vessels to changes in blood flow.

DISCUSSION

Here, we describe a unique role of Piezo1 in activating ER Ca^{2+} release that plays a fundamental role in the adaptation of ECs to shear stresses (as described in the graphic abstract). The data presented here show that the activation of Piezo1 by the application of transient or continuous laminar shear stresses (data not shown) not only induces Ca^{2+} entry from the extracellular milieu into the cytosol but also activates rapid mobilization of Ca^{2+} into the ER lumen in a force-dependent manner. The latter event is followed by a rapid ER Ca^{2+} release from cAMP-sensitive IP_3R2 stores, allowing the amplification and propagation of calcium signaling throughout the cytosol to induce the adaptive response of ECs to shear applied. Thus, Piezo1 regulates flow-induced increases in cytosolic Ca^{2+} by two independent

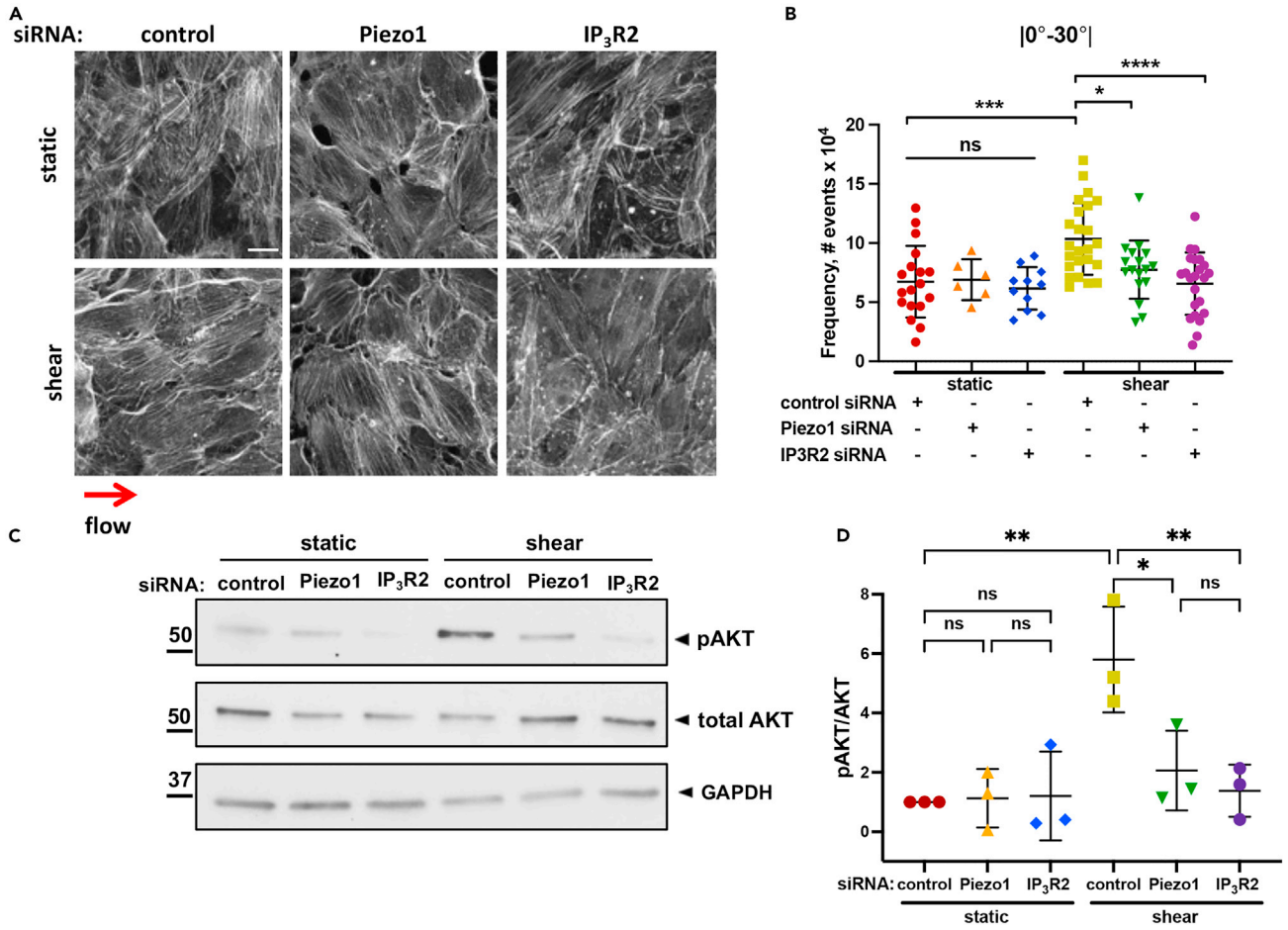

Figure 5. IP_3R2-evoked ER Ca^{2+} release is required for shear-induced EC alignment and activation of Akt

(A) Representative images of F-actin in endothelial monolayers depleted of indicated proteins and grown under static or 10 dyn/cm^2 laminar shear flow conditions for 24 h; red arrow indicates the direction of flow; scale bar 20 μm.

(B) Frequency of F-actin distribution within 0-30° relative to the direction of flow, a measure of cell alignment; n = 6-15 field per condition, from 2 to 4 independent experiment on static group and 17-24 fields per condition from 4 independent experiments on shear group; mean ± SD; *, $p < 0.05$; ***, $p < 0.001$; ****, $p < 0.0001$, ANOVA with Tukey's post hoc test.

(C) Western blot analysis of Akt (Ser 473) phosphorylation in endothelial monolayers depleted of indicated proteins and subjected to static or 10 dyn/cm^2 shear stress conditions for 30 min.

(D) Fold increase in Akt phosphorylation in (C); data are presented as 3 biological replicates from 3 independent experiments; mean ± SD; *, $p < 0.05$; **, $p < 0.01$; ANOVA with Tukey's post hoc test.

mechanisms: through the initial Ca^{2+} mobilization from the extracellular milieu and the release of Ca^{2+} through cAMP-sensitive stores.

The initial Ca^{2+} ions entering through the Piezo1 channel are promptly mobilized into the ER lumen by SERCA, the Ca^{2+} pump that recycles cytosolic Ca^{2+} into the ER lumen.[43] ECs express all mammalian SERCA isoforms, including SERCA2a and SERCA3,[44] which exhibit high Ca^{2+} turnover rates[45,46] and might be involved in regulating the rapid mobilization of Ca^{2+} into the ER lumen downstream of Piezo1 mechanosensing. We speculate that the activation of Piezo1, which forms a complex with all SERCA isoforms to inhibit their activity,[24] may modulate SERCA function by relieving the inhibitory effects on SERCA activity.[24] The rapid kinetics of Ca^{2+} mobilization into the ER also suggests that Piezo1 might be recruited to specific plasma membrane microdomains to form a transient interaction with the ER membrane. Therefore, we posit that Piezo1-mediated mobilization of Ca^{2+} into the ER resembles the STIM1-Orai pathway, which refills the ER stores.[31] In the latter case, SERCA is recruited to STIM1 and Orai clusters[47,48] to pump Ca^{2+} into the ER lumen upon the influx of extracellular Ca^{2+} through Orai.[49]

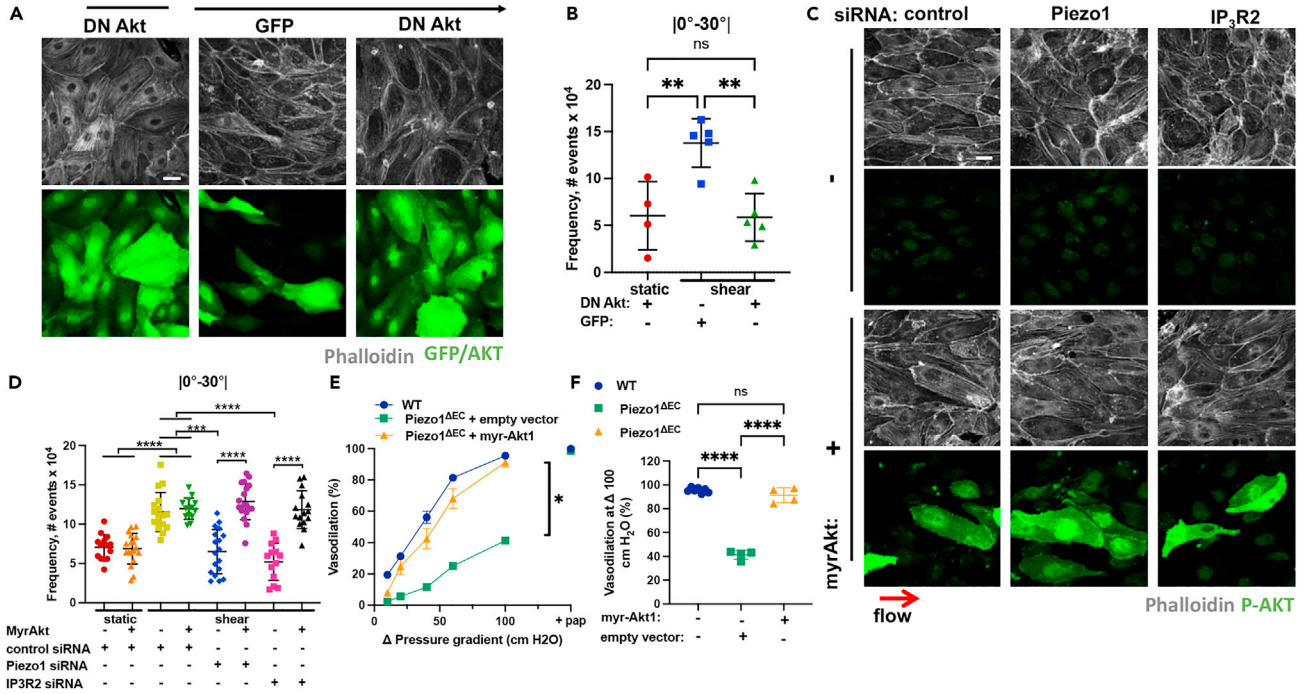

Figure 6. Activation of Akt downstream of Piezo1-sAC-IP$_3$R2 circuit is required for the adaptation of endothelial cells to laminar shear stress and vasodilation

(A) Representative images of F-actin, GFP, and Akt in endothelial monolayers ectopically expressing GFP or activity deficient AD-Akt. Cells were grown at static or 10 dyn/cm^2 laminar shear stress conditions for 24 h; red arrow indicates the direction of flow; scale bar 20 μm.

(B) Frequency of F-actin distribution within 0-30° angle relative to the direction of flow in (A); n = 5-10 fields per condition from 2 independent experiments; mean ± SD; **, $p < 0.01$, ANOVA with Tukey's post hoc test.

(C) Representative images of F-actin and phospho-Akt (*p*-Akt) in endothelial monolayers depleted of Piezo1 or IP$_3$R2 and ectopically expressing empty vector or myr-Akt1. Cells were grown at static or 10 dyn/cm^2 laminar shear stress conditions for 24 h; ref arrows indicate the direction of flow; scale bar 20 μm.

(D) Frequency of F-actin distribution within 0-30° angle relative to the direction of flow; n = 14-18 fields per condition across 3 independent experiments; mean ± SD; ***, $p < 0.001$; ****, $p < 0.0001$, ANOVA with Tukey's post hoc test.

(E) Flow-induced vasodilation of mesenteric arteries isolated from wild type (WT) or Piezo1$^{\Delta EC}$ mice infected with adenoviral particles encoding empty vector or myr-Akt1 as indicated. n = 4 and 7 for Piezo1$^{\Delta EC}$ and WT mice, respectively; *, $p < 0.05$ using two-way ANOVA, pap: papaverine.

(F) Quantification of data in (E) at Δ100 cm H_2O; ****, $p < 0.0001$, ANOVA with Tukey's post hoc test.

However, Piezo1 induces prompt mobilization of extracellular Ca^{2+} into the ER through the activation of SERCA. The present findings also show functional differences by which Orai and Piezo1 operate to mediate extracellular Ca^{2+} influx. While Orai is activated by STIM1 upon ER store depletion,[30,31,50] rapid mobilization of Ca^{2+} in the ER downstream of Piezo1 is activated by mechanical stimuli independent of ER store depletion. We show that STIM1 is dispensable for the initial rapid mobilization of extracellular Ca^{2+} into the ER but is involved in ER Ca^{2+} replenishment secondary to IP$_3$R2-evoked Ca^{2+} release downstream of Piezo1 mechanosensing.

ER Ca^{2+} storage accounts for 75% of intracellular Ca^{2+} in ECs.[51] The build-up of ER Ca^{2+} can influence the sensitivity of IP$_3$R and RyR channels to their ligands[35,52] and concomitantly activate ER Ca^{2+} release. The ER Ca^{2+} release downstream of Piezo1 described here was independent of the initial increase in luminal ER Ca^{2+}. Treatment of cells with thapsigargin, a potent inhibitor of SERCA, blocked Ca^{2+} uptake into the ER lumen but did not alter the kinetics of ER Ca^{2+} decay downstream of Piezo1 activation. Further analysis of the pathways involved in ER Ca^{2+} release revealed that Piezo1-mediated influx of extracellular Ca^{2+} subsequently activated ER Ca^{2+} release into the cytosol through the IP$_3$R2 channel. This rapid ER Ca^{2+} release was an essential part of the mechanotransduction response required for rapid increase in cytosolic Ca^{2+}.

In contrast to IP$_3$R3, which is activated by IP$_3$ and free intracellular Ca^{2+}, IP$_3$R2 activity can be potentiated by cAMP.[53,54] Production of both cAMP and ATP are commonly induced by mechanical forces, including shear

stresses.[55,56] We show that the activation of Piezo1 with Yoda1 induced a transient increase in cAMP production. Depletion of sAC suppressed the Piezo1-mediated increase in cAMP, consistent with the crucial role of sAC, which is activated by free intracellular Ca^{2+},[39] in the generation of cAMP and cAMP-dependent ER Ca^{2+} release downstream of Piezo1 mechanosensing. cAMP potentiates IP_3-evoked Ca^{2+} release by unmasking hypersensitive IP_3R2 channels and potentiates IP_3-evoked Ca^{2+} release from a discrete ER Ca^{2+} stores.[54] We speculate that Piezo1 downstream signaling is spatially controlled and restricted to a subset of IP_3R2, which has a distinct intracellular distribution compared to IP_3R3 precluding the activation of calcium-induced calcium release from IP_3R3 stores. cAMP may also induce Ca^{2+} release by phosphorylating all IP_3Rs including IP_3R3 in a PKA-dependent manner[57]; however, this mechanism does not explain our results because the depletion of IP_3R3 had no effect on ER Ca^{2+} release. Thus, our data support the role of the cAMP-IP_3R2 pathway, consistent with the specific effect of cAMP on IP_3R2 channels.[53,54] sAC tethered to the mitochondria and microtubules[58] can generate cAMP in close proximity to IP_3R2, which localizes at ER-mitochondrial interaction sites.[59] Therefore, the subcellular organization of cAMP signals[60,61] distinguishes the functional role of sAC from the transmembrane AC1, AC3, and AC8 isoforms that are also activated by Ca^{2+} signaling through binding to calmodulin.[62]

Transient receptor potential cation channel V4 (TRPV4) also contributes to shear-evoked Ca^{2+} mobilization.[18,63] Deletion of the *Trpv4* gene significantly reduces shear-induced Ca^{2+} influx in ECs and vasodilation of small mesenteric arteries in mice.[63] Recent work showed that TRPV4 activation might be coupled to Piezo1 signaling.[64,65] Therefore, our results describing the mechanism of IP_3R2 activation downstream of Piezo1 may also inform how Piezo1 induced Ca^{2+} mobilization contributes to consequent activation of TRPV4 by shear stresses.[63] We posit here that release of ER Ca^{2+} through sAC-sensitive IP_3R2 stores can play an essential role in the amplification of calcium signaling downstream of Piezo1, a fast-inactivating channel,[16] which cannot produce, as we show here, a sufficient increase in cytosolic calcium to activate EC response to shear stress. It is possible that IP_3R2-evoked release is required for the activation of phospholipase A (PLA2), which is responsible for the generation of 5′,6′-epoxyeicosatrienoic acid from arachidonic acid[66,67] and the sequential activation of TRPV4 by this natural ligand.[64]

ECs exposed to laminar shear stress undergo adaptive morphological changes through the reorientation of cells parallel to the direction of flow.[68] Our findings show that these changes rely on a Piezo1-mediated increase in cytosolic Ca^{2+} since ECs lacking Piezo1 failed to adapt to shear stress[18] and induce flow-mediated vasodilation.[69] We demonstrate here that the genetic ablation of IP_3R2 or sAC not only mitigate the increase in cytosolic Ca^{2+} but also prevents the alignment of ECs in the direction of flow, emphasizing the importance of the sAC-IP_3R2 pathway in signaling the adaptive changes of ECs. Strikingly, ectopic expression of myr-Akt1 restores the morphological response of Piezo1- and IP_3R2-deficient cells as well as flow-induced vasodilation of mesenteric vessels of $Piezo1^{\Delta EC}$ mice, showing the critical role of Akt signaling in the shear-induced regulation of vascular tone.

The serine-threonine protein kinase Akt plays a crucial role in integrin-mediated signaling, endothelial cell survival, and endothelial response to laminar shear.[70–72] Akt translocates from the perinuclear region to the upstream edge of cell-cell junctions relative to flow,[73] where it phosphorylated immunoglobulin and proline-rich receptor-1 (IGPR-1) at S220, causing a lateral redistribution of IGPR-1 along the cell-cell junctions parallel to the direction of flow.[74] In our studies, loss of either Piezo1 or IP_3R2 prevented phosphorylation of Akt at S473 in response to shear stresses. Thus, ER Ca^{2+} release was required to activate Akt signaling mediated by sequential phosphorylation at Thr308 and S473 by phosphoinositide-dependent kinases PDK1 and PDK2, and integrin-linked kinase (ILK), respectively.[75,76] Whereas the mechanism of ER Ca^{2+} release in activating Akt signaling remains unclear, shear-induced activation of Akt was essential for the formation of a mechanosensory complex between platelet-endothelial cell adhesion molecule 1 (PECAM1), vascular endothelial (VE)-cadherin, and vascular endothelial growth factor receptors VEGFR2/VEGFR3.[77] In addition, Akt might promote Piezo1 localization at the plasma membrane microdomains, thus providing a positive feedback regulation of Piezo1 mechanosensing.[78] However, the data presented here show that expression of constitutively active Akt1 suffices to restore EC response to shear stress even in absence of Piezo1 or IP_3R2.

The results described here suggest a unique sAC-IP_3R2 signaling pathway activated downstream of Piezo1 mechanosensing in ECs. We propose Piezo1 acts as an essential adaptive sensor for ECs that reorient ECs through regulating ER Ca^{2+} dynamics and Akt signaling.

Limitations of the study

The current study addresses a key signaling mechanism downstream of Piezo1 mechanosensing that promotes EC adaptation to physiological shear stresses using cell culture and *ex vivo* vessel models. A potential limitation to the findings described here is a lack of analyses of the sAC-IP_3R2 pathway in regulating blood pressure, a physiologically relevant response of blood vessels to local and temporal changes in shear stresses *in vivo*. From this perspective, it will be important to investigate the role of the sAC-IP_3R2 pathway using transgenic mouse models allowing a deletion of sAC or IP_3R2 in ECs. On the basis of our findings, it is anticipated that similar to Piezo1 EC-KO mice,[22] animals deficient of sAC or IP_3R2 in endothelial cells would be prone to hypertension.

STAR★METHODS

Detailed methods are provided in the online version of this paper and include the following:

- KEY RESOURCES TABLE
- RESOURCE AVAILABILITY
  - Lead contact
  - Materials availability
  - Data and code availability
- EXPERIMENTAL MODEL AND SUBJECT DETAILS
  - Cell culture
- METHOD DETAILS
  - Transfections
  - Measurements of intracellular calcium
  - Measurement of ER calcium
  - Measurement of cAMP production
  - Shear stress
  - Immunofluorescent staining and image analysis
  - Western blotting analysis
  - Curve fit and quantification of rate constants
  - Vasodilation measurement in mouse mesenteric arteries
- QUANTIFICATION AND STATISTICAL ANALYSIS

SUPPLEMENTAL INFORMATION

Supplemental information can be found online at https://doi.org/10.1016/j.isci.2023.106661.

ACKNOWLEDGMENTS

This work made use of Confocal Microscopy Facility (Research Resources Center, UIC). The authors would like to thank Jae-Won Shin for suggestions related to the analysis of calcium kinetics. The work is supported by NHLBI grants T32HL007829, and R01HL045638 and R01HL045638 supplement.

AUTHOR CONTRIBUTIONS

YAK and *DS* designed research studies, *DS, SJA, and ACM* conducted experiments and acquired data; *DL* assisted with flow experiments, *YAK, QL, SJA, and DS* analyzed and interpreted data; *YAK* and *DS* wrote the article. *DM, IL,* and *ABM* provided feedback and discussion of the data and edited the article.

DECLARATION OF INTERESTS

The authors have declared that no conflict of interest exists.

INCLUSION AND DIVERSITY

We support inclusive, diverse, and equitable conduct of research.

Received: August 22, 2022
Revised: January 30, 2023
Accepted: April 7, 2023
Published: April 11, 2023

REFERENCES

1. Dewey, C.F., Jr., Bussolari, S.R., Gimbrone, M.A., Jr., and Davies, P.F. (1981). The dynamic response of vascular endothelial cells to fluid shear stress. J. Biomech. Eng. *103*, 177–185. https://doi.org/10.1115/1.3138276.

2. Davies, P.F. (2009). Hemodynamic shear stress and the endothelium in cardiovascular pathophysiology. Nat. Clin. Pract. Cardiovasc. Med. *6*, 16–26. https://doi.org/10.1038/ncpcardio1397.

3. Schwartz, E.A., Bizios, R., Medow, M.S., and Gerritsen, M.E. (1999). Exposure of human vascular endothelial cells to sustained hydrostatic pressure stimulates proliferation. Circ. Res. *84*, 315–322. https://doi.org/10.1161/01.RES.84.3.315.

4. Acevedo, A.D., Bowser, S.S., Gerritsen, M.E., and Bizios, R. (1993). Morphological and proliferative responses of endothelial cells to hydrostatic pressure: role of fibroblast growth factor. J. Cell. Physiol. *157*, 603–614. https://doi.org/10.1002/jcp.1041570321.

5. Awolesi, M.A., Sessa, W.C., and Sumpio, B.E. (1995). Cyclic strain upregulates nitric oxide synthase in cultured bovine aortic endothelial cells. J. Clin. Invest. *96*, 1449–1454. https://doi.org/10.1172/JCI118181.

6. Galie, P.A., Nguyen, D.H.T., Choi, C.K., Cohen, D.M., Janmey, P.A., and Chen, C.S. (2014). Fluid shear stress threshold regulates angiogenic sprouting. Proc. Natl. Acad. Sci. USA *111*, 7968–7973. https://doi.org/10.1073/pnas.1310842111.

7. Cunningham, K.S., and Gotlieb, A.I. (2005). The role of shear stress in the pathogenesis of atherosclerosis. Lab. Invest. *85*, 9–23. https://doi.org/10.1038/labinvest.3700215.

8. Huo, Y., Linares, C.O., and Kassab, G.S. (2007). Capillary perfusion and wall shear stress are restored in the coronary circulation of hypertrophic right ventricle. Circ. Res. *100*, 273–283. https://doi.org/10.1161/01.Res.0000257777.83431.13.

9. Mairey, E., Genovesio, A., Donnadieu, E., Bernard, C., Jaubert, F., Pinard, E., Seylaz, J., Olivo-Marin, J.C., Nassif, X., and Duménil, G. (2006). Cerebral microcirculation shear stress levels determine Neisseria meningitidis attachment sites along the blood-brain barrier. J. Exp. Med. *203*, 1939–1950. https://doi.org/10.1084/jem.20060482.

10. Garcia-Polite, F., Martorell, J., Del Rey-Puech, P., Melgar-Lesmes, P., O'Brien, C.C., Roquer, J., Ois, A., Principe, A., Edelman, E.R., and Balcells, M. (2017). Pulsatility and high shear stress deteriorate barrier phenotype in brain microvascular endothelium. J. Cerebr. Blood Flow Metabol. *37*, 2614–2625. https://doi.org/10.1177/0271678x16672482.

11. Chachisvilis, M., Zhang, Y.-L., and Frangos, J.A. (2006). G protein-coupled receptors sense fluid shear stress in endothelial cells. Proc. Natl. Acad. Sci. USA *103*, 15463–15468. https://doi.org/10.1073/pnas.0607224103.

12. Xu, J., Mathur, J., Vessières, E., Hammack, S., Nonomura, K., Favre, J., Grimaud, L., Petrus, M., Francisco, A., Li, J., et al. (2018). GPR68 senses flow and is essential for vascular Physiology. Cell *173*, 762–775.e16. https://doi.org/10.1016/j.cell.2018.03.076.

13. Noria, S., Cowan, D.B., Gotlieb, A.I., and Langille, B.L. (1999). Transient and steady-state effects of shear stress on endothelial cell adherens junctions. Circ. Res. *85*, 504–514. https://doi.org/10.1161/01.RES.85.6.504.

14. Langille, B.L. (2001). Morphologic responses of endothelium to shear stress: reorganization of the adherens junction. Microcirculation *8*, 195–206. https://doi.org/10.1038/sj/mn/7800085.

15. Watanabe, H., Vriens, J., Janssens, A., Wondergem, R., Droogmans, G., and Nilius, B. (2003). Modulation of TRPV4 gating by intra- and extracellular Ca2+. Cell Calcium *33*, 489–495. https://doi.org/10.1016/s0143-4160(03)00064-2.

16. Coste, B., Mathur, J., Schmidt, M., Earley, T.J., Ranade, S., Petrus, M.J., Dubin, A.E., and Patapoutian, A. (2010). Piezo1 and Piezo2 are essential components of distinct mechanically activated cation channels. Science *330*, 55–60. https://doi.org/10.1126/science.1193270.

17. Gerhold, K.A., and Schwartz, M.A. (2016). Ion channels in endothelial responses to fluid shear stress. Physiology *31*, 359–369. https://doi.org/10.1152/physiol.00007.2016.

18. Li, J., Hou, B., Tumova, S., Muraki, K., Bruns, A., Ludlow, M.J., Sedo, A., Hyman, A.J., McKeown, L., Young, R.S., et al. (2014). Piezo1 integration of vascular architecture with physiological force. Nature *515*, 279–282. https://doi.org/10.1038/nature13701.

19. Ranade, S.S., Qiu, Z., Woo, S.H., Hur, S.S., Murthy, S.E., Cahalan, S.M., Xu, J., Mathur, J., Bandell, M., Coste, B., et al. (2014). Piezo1, a mechanically activated ion channel, is required for vascular development in mice. Proc. Natl. Acad. Sci. USA *111*, 10347–10352. https://doi.org/10.1073/pnas.1409233111.

20. Friedrich, E.E., Hong, Z., Xiong, S., Zhong, M., Di, A., Rehman, J., Komarova, Y.A., and Malik, A.B. (2019). Endothelial cell Piezo1 mediates pressure-induced lung vascular hyperpermeability via disruption of adherens junctions. Proc. Natl. Acad. Sci. USA *116*, 12980–12985. https://doi.org/10.1073/pnas.1902165116.

21. Duchemin, A.-L., Vignes, H., and Vermot, J. (2019). Mechanically activated piezo channels modulate outflow tract valve development through the Yap1 and Klf2-Notch signaling axis. Elife *8*, e44706.

22. Wang, S., Chennupati, R., Kaur, H., Iring, A., Wettschureck, N., and Offermanns, S. (2016). Endothelial cation channel PIEZO1 controls blood pressure by mediating flow-induced ATP release. J. Clin. Invest. *126*, 4527–4536. https://doi.org/10.1172/JCI87343.

23. Nollert, M.U., Eskin, S.G., and McIntire, L.V. (1990). Shear stress increases inositol trisphosphate levels in human endothelial cells. Biochem. Biophys. Res. Commun. *170*, 281–287. https://doi.org/10.1016/0006-291x(90)91271-s.

24. Zhang, T., Chi, S., Jiang, F., Zhao, Q., and Xiao, B. (2017). A protein interaction mechanism for suppressing the mechanosensitive Piezo channels. Nat. Commun. *8*, 1797. https://doi.org/10.1038/s41467-017-01712-z.

25. Majerus, P.W., Connolly, T.M., Deckmyn, H., Ross, T.S., Bross, T.E., Ishii, H., Bansal, V.S., and Wilson, D.B. (1986). The metabolism of phosphoinositide-derived messenger molecules. Science *234*, 1519–1526.

26. Rebecchi, M.J., and Pentyala, S.N. (2000). Structure, function, and control of phosphoinositide-specific phospholipase C. Physiol. Rev. *80*, 1291–1335.

27. Suzuki, J., Kanemaru, K., Ishii, K., Ohkura, M., Okubo, Y., and Iino, M. (2014). Imaging intraorganellar Ca2+ at subcellular resolution using CEPIA. Nat. Commun. *5*, 4153. https://doi.org/10.1038/ncomms5153.

28. Syeda, R., Xu, J., Dubin, A.E., Coste, B., Mathur, J., Huynh, T., Matzen, J., Lao, J., Tully, D.C., Engels, I.H., et al. (2015). Chemical activation of the mechanotransduction channel Piezo1. Elife *4*, e07369. https://doi.org/10.7554/eLife.07369.

29. Hofmann, T., Obukhov, A.G., Schaefer, M., Harteneck, C., Gudermann, T., and Schultz, G. (1999). Direct activation of human TRPC6 and TRPC3 channels by diacylglycerol. Nature *397*, 259–263. https://doi.org/10.1038/16711.

30. Xu, P., Lu, J., Li, Z., Yu, X., Chen, L., and Xu, T. (2006). Aggregation of STIM1 underneath the plasma membrane induces clustering of Orai1. Biochem. Biophys. Res. Commun. *350*, 969–976. https://doi.org/10.1016/j.bbrc.2006.09.134.

31. Calloway, N., Vig, M., Kinet, J.P., Holowka, D., and Baird, B. (2009). Molecular clustering of STIM1 with Orai1/CRACM1 at the plasma membrane depends dynamically on depletion of Ca2+ stores and on electrostatic interactions. Mol. Biol. Cell *20*, 389–399. https://doi.org/10.1091/mbc.e07-11-1132.

32. Thastrup, O., Cullen, P.J., Drøbak, B.K., Hanley, M.R., and Dawson, A.P. (1990). Thapsigargin, a tumor promoter, discharges intracellular Ca2+ stores by specific inhibition of the endoplasmic reticulum Ca2(+)-ATPase. Proc. Natl. Acad. Sci. USA *87*, 2466–2470. https://doi.org/10.1073/pnas.87.7.2466.

33. Foskett, J.K., White, C., Cheung, K.H., and Mak, D.O.D. (2007). Inositol trisphosphate receptor Ca2+ release channels. Physiol. Rev. *87*, 593–658. https://doi.org/10.1152/physrev.00035.2006.

34. Geyer, M., Huang, F., Sun, Y., Vogel, S.M., Malik, A.B., Taylor, C.W., and Komarova, Y.A. (2015). Microtubule-associated protein EB3 regulates IP3 receptor clustering and Ca(2+) signaling in endothelial cells. Cell Rep. *12*,

79–89. https://doi.org/10.1016/j.celrep.2015.06.001.

35. Finch, E.A., Turner, T.J., and Goldin, S.M. (1991). Calcium as a coagonist of inositol 1,4,5-trisphosphate-induced calcium release. Science *252*, 443–446. https://doi.org/10.1126/science.2017683.

36. Tovey, S.C., Dedos, S.G., Rahman, T., Taylor, E.J.A., Pantazaka, E., and Taylor, C.W. (2010). Regulation of inositol 1,4,5-trisphosphate receptors by cAMP independent of cAMP-dependent protein kinase. J. Biol. Chem. *285*, 12979–12989. https://doi.org/10.1074/jbc.M109.096016.

37. Taylor, C.W. (2017). Regulation of IP(3) receptors by cyclic AMP. Cell Calcium *63*, 48–52. https://doi.org/10.1016/j.ceca.2016.10.005.

38. Abdullaev, I.F., Bisaillon, J.M., Potier, M., Gonzalez, J.C., Motiani, R.K., and Trebak, M. (2008). Stim1 and Orai1 mediate CRAC currents and store-operated calcium entry important for endothelial cell proliferation. Circ. Res. *103*, 1289–1299. https://doi.org/10.1161/01.Res.0000338496.95579.56.

39. Litvin, T.N., Kamenetsky, M., Zarifyan, A., Buck, J., and Levin, L.R. (2003). Kinetic properties of "soluble" adenylyl cyclase. Synergism between calcium and bicarbonate. J. Biol. Chem. *278*, 15922–15926. https://doi.org/10.1074/jbc.M212475200.

40. Tewson, P.H., Martinka, S., Shaner, N.C., Hughes, T.E., and Quinn, A.M. (2016). New DAG and cAMP sensors optimized for live-cell assays in automated laboratories. J. Biomol. Screen *21*, 298–305. https://doi.org/10.1177/1087057115618608.

41. Alessi, D.R., Andjelkovic, M., Caudwell, B., Cron, P., Morrice, N., Cohen, P., and Hemmings, B.A. (1996). Mechanism of activation of protein kinase B by insulin and IGF-1. EMBO J. *15*, 6541–6551.

42. Fulton, D., Gratton, J.P., McCabe, T.J., Fontana, J., Fujio, Y., Walsh, K., Franke, T.F., Papapetropoulos, A., and Sessa, W.C. (1999). Regulation of endothelium-derived nitric oxide production by the protein kinase Akt. Nature *399*, 597–601. https://doi.org/10.1038/21218.

43. Brini, M., and Carafoli, E. (2009). Calcium pumps in health and disease. Physiol. Rev. *89*, 1341–1378. https://doi.org/10.1152/physrev.00032.2008.

44. Mountian, I., Manolopoulos, V.G., De Smedt, H., Parys, J.B., Missiaen, L., and Wuytack, F. (1999). Expression patterns of sarco/endoplasmic reticulum Ca(2+)-ATPase and inositol 1,4,5-trisphosphate receptor isoforms in vascular endothelial cells. Cell Calcium *25*, 371–380. https://doi.org/10.1054/ceca.1999.0034.

45. Verboomen, H., Wuytack, F., De Smedt, H., Himpens, B., and Casteels, R. (1992). Functional difference between SERCA2a and SERCA2b Ca2+ pumps and their modulation by phospholamban. Biochem. J. *286*, 591–595. https://doi.org/10.1042/bj2860591.

46. Dode, L., Andersen, J.P., Leslie, N., Dhitavat, J., Vilsen, B., and Hovnanian, A. (2003). Dissection of the functional differences between sarco(endo)plasmic reticulum Ca2+-ATPase (SERCA) 1 and 2 isoforms and characterization of Darier disease (SERCA2) mutants by steady-state and transient kinetic analyses. J. Biol. Chem. *278*, 47877–47889. https://doi.org/10.1074/jbc.M306784200.

47. Jousset, H., Frieden, M., and Demaurex, N. (2007). STIM1 knockdown reveals that store-operated Ca2+ channels located close to sarco/endoplasmic Ca2+ ATPases (SERCA) pumps silently refill the endoplasmic reticulum. J. Biol. Chem. *282*, 11456–11464. https://doi.org/10.1074/jbc.M609551200.

48. Manjarrés, I.M., Rodríguez-García, A., Alonso, M.T., and García-Sancho, J. (2010). The sarco/endoplasmic reticulum Ca(2+) ATPase (SERCA) is the third element in capacitative calcium entry. Cell Calcium *47*, 412–418. https://doi.org/10.1016/j.ceca.2010.03.001.

49. Alonso, M.T., Manjarrés, I.M., and García-Sancho, J. (2012). Privileged coupling between Ca(2+) entry through plasma membrane store-operated Ca(2+) channels and the endoplasmic reticulum Ca(2+) pump. Mol. Cell. Endocrinol. *353*, 37–44. https://doi.org/10.1016/j.mce.2011.08.021.

50. Liou, J., Kim, M.L., Heo, W.D., Jones, J.T., Myers, J.W., Ferrell, J.E., Jr., and Meyer, T. (2005). STIM is a Ca2+ sensor essential for Ca2+-store-depletion-triggered Ca2+ influx. Curr. Biol. *15*, 1235–1241. https://doi.org/10.1016/j.cub.2005.05.055.

51. Tran, Q.K., Ohashi, K., and Watanabe, H. (2000). Calcium signalling in endothelial cells. Cardiovasc. Res. *48*, 13–22. https://doi.org/10.1016/s0008-6363(00)00172-3.

52. Meissner, G. (1994). Ryanodine receptor/Ca2+ release channels and their regulation by endogenous effectors. Annu. Rev. Physiol. *56*, 485–508.

53. Tovey, S.C., Dedos, S.G., Taylor, E.J.A., Church, J.E., and Taylor, C.W. (2008). Selective coupling of type 6 adenylyl cyclase with type 2 IP3 receptors mediates direct sensitization of IP3 receptors by cAMP. J. Cell Biol. *183*, 297–311. https://doi.org/10.1083/jcb.200803172.

54. Konieczny, V., Tovey, S.C., Mataragka, S., Prole, D.L., and Taylor, C.W. (2017). Cyclic AMP recruits a discrete intracellular Ca(2+) store by unmasking hypersensitive IP(3) receptors. Cell Rep. *18*, 711–722. https://doi.org/10.1016/j.celrep.2016.12.058.

55. Reich, K.M., Gay, C.V., and Frangos, J.A. (1990). Fluid shear stress as a mediator of osteoblast cyclic adenosine monophosphate production. J. Cell. Physiol. *143*, 100–104. https://doi.org/10.1002/jcp.1041430113.

56. Yamamoto, K., Furuya, K., Nakamura, M., Kobatake, E., Sokabe, M., and Ando, J. (2011). Visualization of flow-induced ATP release and triggering of Ca2+ waves at caveolae in vascular endothelial cells. J. Cell Sci. *124*, 3477–3483. https://doi.org/10.1242/jcs.087221.

57. Wojcikiewicz, R.J., and Luo, S.G. (1998). Phosphorylation of inositol 1,4,5-trisphosphate receptors by cAMP-dependent protein kinase. Type I, II, and III receptors are differentially susceptible to phosphorylation and are phosphorylated in intact cells. J. Biol. Chem. *273*, 5670–5677. https://doi.org/10.1074/jbc.273.10.5670.

58. Zippin, J.H., Chen, Y., Nahirney, P., Kamenetsky, M., Wuttke, M.S., Fischman, D.A., Levin, L.R., and Buck, J. (2003). Compartmentalization of bicarbonate-sensitive adenylyl cyclase in distinct signaling microdomains. FASEB J. *17*, 82–84. https://doi.org/10.1096/fj.02-0598fje.

59. Bartok, A., Weaver, D., Golenár, T., Nichtova, Z., Katona, M., Bánsághi, S., Alzayady, K.J., Thomas, V.K., Ando, H., Mikoshiba, K., et al. (2019). IP(3) receptor isoforms differently regulate ER-mitochondrial contacts and local calcium transfer. Nat. Commun. *10*, 3726. https://doi.org/10.1038/s41467-019-11646-3.

60. Valsecchi, F., Konrad, C., D'Aurelio, M., Ramos-Espiritu, L.S., Stepanova, A., Burstein, S.R., Galkin, A., Magranè, J., Starkov, A., Buck, J., et al. (2017). Distinct intracellular sAC-cAMP domains regulate ER Ca(2+) signaling and OXPHOS function. J. Cell Sci. *130*, 3713–3727. https://doi.org/10.1242/jcs.206318.

61. Mewes, M., Lenders, M., Stappers, F., Scharnetzki, D., Nedele, J., Fels, J., Wedlich-Söldner, R., Brand, S.M., Schmitz, B., and Brand, E. (2019). Soluble adenylyl cyclase (sAC) regulates calcium signaling in the vascular endothelium. FASEB J. *33*, 13762–13774. https://doi.org/10.1096/fj.201900724R.

62. Halls, M.L., and Cooper, D.M.F. (2011). Regulation by Ca2+-signaling pathways of adenylyl cyclases. Cold Spring Harb. Perspect. Biol. *3*, a004143. https://doi.org/10.1101/cshperspect.a004143.

63. Mendoza, S.A., Fang, J., Gutterman, D.D., Wilcox, D.A., Bubolz, A.H., Li, R., Suzuki, M., and Zhang, D.X. (2010). TRPV4-mediated endothelial Ca2+ influx and vasodilation in response to shear stress. Am. J. Physiol. Heart Circ. Physiol. *298*, H466–H476. https://doi.org/10.1152/ajpheart.00854.2009.

64. Swain, S.M., and Liddle, R.A. (2021). Piezo1 acts upstream of TRPV4 to induce pathological changes in endothelial cells due to shear stress. J. Biol. Chem. *296*, 100171. https://doi.org/10.1074/jbc.RA120.015059.

65. Swain, S.M., Romac, J.M.J., Shahid, R.A., Pandol, S.J., Liedtke, W., Vigna, S.R., and Liddle, R.A. (2020). TRPV4 channel opening mediates pressure-induced pancreatitis initiated by Piezo1 activation. J. Clin. Invest. *130*, 2527–2541. https://doi.org/10.1172/JCI134111.

66. Loot, A.E., Popp, R., Fisslthaler, B., Vriens, J., Nilius, B., and Fleming, I. (2008). Role of cytochrome P450-dependent transient receptor potential V4 activation in flow-induced vasodilatation. Cardiovasc. Res. *80*, 445–452.

67. Watanabe, H., Vriens, J., Prenen, J., Droogmans, G., Voets, T., and Nilius, B. (2003). Anandamide and arachidonic acid use epoxyeicosatrienoic acids to activate TRPV4 channels. Nature *424*, 434–438.

68. Davies, P.F. (1995). Flow-mediated endothelial mechanotransduction. Physiol. Rev. *75*, 519–560. https://doi.org/10.1152/physrev.1995.75.3.519.

69. Albarrán-Juárez, J., Iring, A., Wang, S., Joseph, S., Grimm, M., Strilic, B., Wettschureck, N., Althoff, T.F., and Offermanns, S. (2018). Piezo1 and G(q)/G(11) promote endothelial inflammation depending on flow pattern and integrin activation. J. Exp. Med. *215*, 2655–2672. https://doi.org/10.1084/jem.20180483.

70. Chen, J., Somanath, P.R., Razorenova, O., Chen, W.S., Hay, N., Bornstein, P., and Byzova, T.V. (2005). Akt1 regulates pathological angiogenesis, vascular maturation and permeability in vivo. Nat. Med. *11*, 1188–1196. https://doi.org/10.1038/nm1307.

71. Kobayashi, H., Butler, J.M., O'Donnell, R., Kobayashi, M., Ding, B.S., Bonner, B., Chiu, V.K., Nolan, D.J., Shido, K., Benjamin, L., and Rafii, S. (2010). Angiocrine factors from Akt-activated endothelial cells balance self-renewal and differentiation of haematopoietic stem cells. Nat. Cell Biol. *12*, 1046–1056. https://doi.org/10.1038/ncb2108.

72. Matsuoka, T., Yashiro, M., Nishioka, N., Hirakawa, K., Olden, K., and Roberts, J.D. (2012). PI3K/Akt signalling is required for the attachment and spreading, and growth in vivo of metastatic scirrhous gastric carcinoma. Br. J. Cancer *106*, 1535–1542. https://doi.org/10.1038/bjc.2012.107.

73. Melchior, B., and Frangos, J.A. (2014). Distinctive subcellular Akt-1 responses to shear stress in endothelial cells. J. Cell. Biochem. *115*, 121–129. https://doi.org/10.1002/jcb.24639.

74. Ho, R.X.Y., Tahboub, R., Amraei, R., Meyer, R.D., Varongchayakul, N., Grinstaff, M., and Rahimi, N. (2019). The cell adhesion molecule IGPR-1 is activated by and regulates responses of endothelial cells to shear stress. J. Biol. Chem. *294*, 13671–13680. https://doi.org/10.1074/jbc.RA119.008548.

75. Chan, T.O., and Tsichlis, P.N. (2001). PDK2: a complex tail in one Akt. Sci. STKE *2001*, pe1. https://doi.org/10.1126/stke.2001.66.pe1.

76. Persad, S., Attwell, S., Gray, V., Delcommenne, M., Troussard, A., Sanghera, J., and Dedhar, S. (2000). Inhibition of integrin-linked kinase (ILK) suppresses activation of protein kinase B/Akt and induces cell cycle arrest and apoptosis of PTEN-mutant prostate cancer cells. Proc. Natl. Acad. Sci. USA *97*, 3207–3212. https://doi.org/10.1073/pnas.97.7.3207.

77. Fleming, I., Fisslthaler, B., Dixit, M., and Busse, R. (2005). Role of PECAM-1 in the shear-stress-induced activation of Akt and the endothelial nitric oxide synthase (eNOS) in endothelial cells. J. Cell Sci. *118*, 4103–4111. https://doi.org/10.1242/jcs.02541.

78. Lai, A., Chen, Y.C., Cox, C.D., Jaworowski, A., Peter, K., and Baratchi, S. (2021). Analyzing the shear-induced sensitization of mechanosensitive ion channel Piezo-1 in human aortic endothelial cells. J. Cell. Physiol. *236*, 2976–2987. https://doi.org/10.1002/jcp.30056.

79. Blackman, B.R., García-Cardeña, G., and Gimbrone, M.A., Jr. (2002). A new in vitro model to evaluate differential responses of endothelial cells to simulated arterial shear stress waveforms. J. Biomech. Eng. *124*, 397–407. https://doi.org/10.1115/1.1486468.

80. Dai, G., Kaazempur-Mofrad, M.R., Natarajan, S., Zhang, Y., Vaughn, S., Blackman, B.R., Kamm, R.D., García-Cardeña, G., and Gimbrone, M.A., Jr. (2004). Distinct endothelial phenotypes evoked by arterial waveforms derived from atherosclerosis-susceptible and -resistant regions of human vasculature. Proc. Natl. Acad. Sci. USA *101*, 14871–14876. https://doi.org/10.1073/pnas.0406073101.

81. Ahn, S.J., Fancher, I.S., Bian, J.T., Zhang, C.X., Schwab, S., Gaffin, R., Phillips, S.A., and Levitan, I. (2017). Inwardly rectifying K(+) channels are major contributors to flow-induced vasodilatation in resistance arteries. J. Physiol. *595*, 2339–2364. https://doi.org/10.1113/jp273255.

82. Kruse, K., Lee, Q.S., Sun, Y., Klomp, J., Yang, X., Huang, F., Sun, M.Y., Zhao, S., Hong, Z., Vogel, S.M., et al. (2019). N-cadherin signaling via Trio assembles adherens junctions to restrict endothelial permeability. J. Cell Biol. *218*, 299–316. https://doi.org/10.1083/jcb.201802076.

83. Fonck, E., Feigl, G.G., Fasel, J., Sage, D., Unser, M., Rüfenacht, D.A., and Stergiopulos, N. (2009). Effect of aging on elastin functionality in human cerebral arteries. Stroke *40*, 2552–2556. https://doi.org/10.1161/strokeaha.108.528091.

84. Püspöki, Z., Storath, M., Sage, D., and Unser, M. (2016). Transforms and operators for directional bioimage analysis: a survey. Adv. Anat. Embryol. Cell Biol. *219*, 69–93. https://doi.org/10.1007/978-3-319-28549-8_3.

85. Ahn, S.J., Fancher, I.S., Granados, S.T., Do Couto, N.F., Hwang, C.L., Phillips, S.A., and Levitan, I. (2022). Cholesterol-induced suppression of endothelial kir channels is a driver of impairment of arteriolar flow-induced vasodilation in humans. Hypertension *79*, 126–138. https://doi.org/10.1161/hypertensionaha.121.17672.

STAR★METHODS

KEY RESOURCES TABLE

REAGENT or RESOURCE	SOURCE	IDENTIFIER
Antibodies		
anti-rabbit Piezo1	Biorbyt	orb41297
anti-rabbit IP_3R2	In house against CPDYRDAQNEGKTVRDGELP	NA
Anti-mouse IP_3R3	BD Biosciences	610312; RRID: AB_397704
anti-rabbit sAC	Thermo Fisher	PA5-25756; RRID: AB_2543256
anti-rabbit Stim1	Cell Signaling	4916; RRID: AB_2271287
anti-goat VE-cadherin	Santa Cruz	sc-6458; RRID: AB_2077955
anti-rabbit Total AKT	Cell Signaling	9272S; RRID: AB_329827
anti-rabbit pAKT (p-Ser 473)	Cell Signaling	9271T; RRID: AB_329825
anti-mouse β actin	Santa Cruz	sc47778; RRID: AB_626632
anti-mouse α tubulin	Sigma-Aldrich	T6074; RRID: AB_477582
anti-mouse GAPDH	Proteintech	60004-1-Ig; RRID: AB_2107436
Alexa Fluor 488 Phalloidin	Invitrogen	A12379
anti-mouse GFP	Fisher Scientific	NC9777966
Experimental models: Cell lines		
Human Pulmonary Arterial Endothelial Cells	Lonza	CC-2530, Lot NO:0000662151 CC-2530, Lot NO: 20TL209928
Human Aortic Endothelial Cells	Lonza	CC-2535, Lot NO: 20TL122171
Experimental models: Organisms/strain		
Piezo1 flox/flox	Li et al.[18]	NA
Cdh5-Cre Piezo1 flox/flox	Friedrich et al.[20]	NA
Recombinant DNA		
G-CEPIA1er	Suzuki et al.[27]	Addgene 58215
mCherry-er	Suzuki et al.[27]	NA
myr-Akt	Fulton et al.[42]	NA
AA-Akt	Fulton et al.[42]	NA
pmaxGFP® Vector	Lonza	VPI-1001
Bacterial and virus strains		
Ad-hVECadp-myr-AKT1	Vector Biolabs	N/A
Ad-GFP	Vector Biolabs	#1060
Chemicals, peptides, and recombinant proteins		
EGM2	Lonza	CC-4176
Fibronectin	Sigma-Aldrich	F1141
Dextran from *Leuconostoc mesenteroides*	Millipore-Sigma	D1662
Gene Silencer siRNA Transfection Reagent	Genlantis	T500750
Basic Endothelial Cells Nucleofactor Kit	Lonza	VPI-1001
Fura 2 AM	Life Technologies	F1221
Ionomycin	Life Technologies	I657
$MnCl_2$	Life Technologies	M1787
Calcium Calibration Buffer Kit	Life Technologies	C3008MP

(*Continued on next page*)

Continued

REAGENT or RESOURCE	SOURCE	IDENTIFIER
EC media w/o Phenol Red	Cell Applications	211PR-500
Yoda1	Sigma-Aldrich	SML1558
Bithionol	Selleck Chemicals	S4552
1-Oleoyl-2-acetyl-*sn*-glycerol (OAG)	Sigma-Aldrich	O6754
Thapsigargin	Thermo Fisher	T7458
MINIPULS 3 Peristaltic Pumps	Gilson	
5 m Silicone Tubing 0.8 mm	ibidi	10841
1. 6 mm serial connector for μ-Slides	ibidi	10830
Elbow Luer connector male	ibidi	10802
μ-Slide I 0.2	ibidi	80161
μ-Slide I 0.4	ibidi	80171
μ-Slide VI 0.4	ibidi	80601
Ripa Buffer	Thermo Fisher	R027
Laemmli Sample Buffer	Bio Rad	1610747
Critical commercial assays		
Green Up cADDis cAMP Assay Kit	Montana Molecular	U0200G
BCA Protein Assay Kit	Thermo Fisher	23225
Oligonucleotides		
ON-Targe Plus SMART pool Piezo1 siRNA: GCAGCAUGACAGACGACAU UGGAGUAUGCCAACGAGAA UGGCUGAUGUUGUCGACUU GCGCAUCAGUCUACGUUUU	Horizon Discovery	L-020870-03-0005
ON-Targe Plus SMART pool IP_3R2 siRNA: CGAAAUGGCCGCUCUAUUA GCAAUGGGUUGGAGACUAU GGAAUGAAAGGGCAAUUAA GAGCAAUAACUACCGGAUU	Horizon Discovery	L-006208-02-0005
ITPR3 GCAUGGAGCAGAUCGUGU	Thermo Fischer	4392420
ADCY10 CCAAAGAACUGGACUCGUA	Horizon Discovery	J-006353-09-0005
Silencer Negative Control siRNA #1	Thermo Fischer	AM4635
Software and algorithms		
ImageJ (FIJI)	National Institutes of Health	https://fiji.sc/
Prism 7	Graph Pad	https://www.graphpad.com/scientific-software/prism/

RESOURCE AVAILABILITY

Lead contact

Any additional information and requests for resources and materials should be addressed and will be fulfill by the lead contact, Yulia A. Komarova (ykomarov@uic.edu).

Materials availability

Any request for resources and materials utilized in this paper should be addressed and fulfill by the lead contact, Yulia A. Komarova (ykomarov@uic.edu).

Data and code availability

- All raw data or information related to western blot quantification as well as image analysis presented in this paper is available from the lead contact upon request.
- This paper does not report original code.

- Any additional information required to reanalyze the data reported in this paper is available from the lead contact upon request.

EXPERIMENTAL MODEL AND SUBJECT DETAILS

Cell culture

Human Pulmonary Artery Endothelial cells (cat# CC-2530; Lots: 0000662151 and 20TL209928) and Human Aortic Endothelial cells (Catalog #: CC-2535) purchased from Lonza were grown in EGM-2 media (cat# CC-4176; Lonza) supplemented with EGM2 Bulletkit and 10% fetal bovine serum (FBS). Cells were cultured at 37 with 5% CO_2 and used from passages 4–7.

METHOD DETAILS

Transfections

Cells were treated with IP_3R2, IP_3R3, Piezo1 and sAC siRNA duplexes using Gene Silencer transfection reagent (cat# T500750; Genlantis) and used for experiments at 72–96 h post-treatment. Cells were transfected with G-CEPIA1er sensor and ER marker mCherry-er[27] by electroporating DNA vectors using Basic Endothelial Cells Nucleofactor Kit (cat# VPI-1001; Lonza) and a Nucleofactor Device (Lonza) according to the manufacturer's instructions. Following DNA electroporation, cells were seeded at 70–75% confluency and confluent monolayers were imaged 24–48 hours post transfection. For cell alignment experiments cells were transfected with myr-Akt and activation deficient AD-Akt.[42] Myr-AKT and AD-AKT constructs were a gift from Dr. Monica Lee's laboratory.

Measurements of intracellular calcium

Intracellular calcium concentrations were measured as previously described by us.[34] HPAE cells grown on glass-bottom dishes (Becton Dickinson) were loaded with 3 μM Fura 2 AM (Life technologies) for 20 minutes at 37°C in EGM-2 media without supplements. Cells were washed with Hank's balanced salt solution (HBSS) containing Ca^{2+} and Mg^{2+} and images were acquired at room temperature in phenol-free media (Cell Applications, cat# 211PR-500). Fura-2 AM fluorescence was excited at 340 and 380 nm and collected at 510 ± 80 nm using an Axiovert 100 inverted microscope (Carl Zeiss) equipped with Plan-Apo 60× with the numerical aperture (NA) 1.4 oil immersion objective, Lambda DG-4 switcher illumination system (Sutter Instruments), AxioCom Hsm camera (Zeiss), fura-2 filter set (Chroma), and AxioVision Physiology Acquisition module. Images were collected at 2-s intervals. Fluorescence ratios (F_{340}/F_{380}) were calculated within a circular region of interest (radius 3 μm) for each cell after subtraction of intracellular background, which was determined after quenching Fura-2 AM fluorescence by adding a mixture of 3 μM ionomycin and 5 mM $MnCl_2$ in HBSS. $[Ca^{2+}]_c$ was calculated from F_{340}/F_{380} ratios using references to Ca^{2+} standard solutions (Calcium Calibration Buffer Kits; Life technologies). Stored Operated Calcium Entry (SOCE) was determined in HPAE cells loaded with Fura 2AM, incubated in Ca^{2+} free HBSS media, and stimulated with 2 μM thapsigargin. Ca^{2+} entry was determined by addition of 2 mM Ca^{2+}.

Measurement of ER calcium

Live-cell images of G-CEPIA1er and mCherry-er[27] were simultaneously acquired at 37°C before and after treatment of HPAECs with 5 μM Yoda1 using a confocal microscope (Zeiss LSM 710, Axio Observer Z1) equipped with a 63× 1.4 NA Plan-Apochromat oil immersion as well as a 10× 0.5 NA Plan-Apochromat dry objectives and a diode-pumped solid-state laser. The 63× objective was used to obtain high resolution images of the ER structure whereas the images in shear stress experiments were acquired with 10× objective to correct for rapid changes in focal plane. Dual-color images were captured simultaneously using λ = 561nm and 488nm lasers and two BiG (binary gallium arsenide phosphide photomultiplier tube (GaAsP-PMT) detectors. For comparisons of relative change in $[Ca^{2+}]_{ER}$, a cross-sectional view intensity values of G-CEPIA1er normalized to mCherry intensity values was generated at each time point, and the relative changes in $[Ca^{2+}]_{ER}$were calculated.

In the experiments with SERCA inhibitor, cells were pretreated with 2 μM thapsigargin prior to starting live-cell imaging experiments to ensure that SERCA is inhibited at the time of Yoda1 treatment without causing a significant decrease in $[Ca^{2+}]_{ER}$.

Measurement of cAMP production

cAMP production was measured using a genetically encoded Green Up cADDis cAMP sensor[40] packed in a BackMam viral vector (Montana Molecular; cat# U0200G), according to the manufacturer's protocol. The changes in cAMP fluorescence upon 5 μM Yoda1 treatment were assessed using a Nikon Eclipse Ti microscope equipped with a 20X/0.40 objective and NIS-Elements image software at 48 hours post-transduction.

Shear stress

For live-cell imaging and immunofluorescent staining experiments, pulsatile laminar shear stress was applied on cells grown on μ-Slide I 0.2, μ-Slide I 0.4 or μ-Slide VI 0.4 to achieve different ranges of shear stress levels (IBIDI, cat# 80161, 80171, and 80601) using a MINIPULS 3 Peristaltic Pump (Gilson) connected with a 1.6 mm serial connector for μ-Slides and elbow luer connector male (IBIDI; cat# 10830 and 10802). Shear stress application was made accordingly to IBIDI shear rate calculation for μ-Slides. For measurements of relative $[Ca^{2+}]_{ER}$, cells were imaged before and after application of 2, 5 or 10 dyn/cm^2 shear stresses for 60 seconds or duration of the experiment (data not shown). For cell alignment assays, cells were subjected to flow or static condition for 24 hours.

For biochemical assessment of Akt signaling, cells were incubated in a 6 well plate and subjected to 10 dyn/cm^2 shear stress for 30 minutes. The laminar shear flow was replicated using a flow device consisting of a cone and plate apparatus describe elsewhere.[79,80] The flow device consisted of a computerized stepper motor UMD-17 (Arcus Technology) and a 1 deg tapered stainless steel cone.[81]

Immunofluorescent staining and image analysis

Immunofluorescent staining was made as published by us.[82] In brief, HPAE cells were fixed with 4% formaldehyde in phosphate buffered saline (PBS) for 10 min at room temperature, washed once with PBS, and permeabilized for 15 min with 0.01% Triton X-100 in PBS. Nonspecific sites were blocked with 3% Bovine Serum Albumin (BSA) solution in PBS for 2 hours at room temperature. Cells were incubated with primary antibody for 1 hour at room temp (or overnight at 4°C). After several washes with PBS, samples were incubated with secondary antibodies for 2 hours at room temperature. Cells were mounted Flouromount-G with DAPI. Images were collected with a confocal microscope (Zeiss LSM880 Confocal Microscope) equipped with a 63× 1.4 NA Plan-Apochromat oil immersion objective.

To analyze the orientation of cells, a z-projected image of samples stained with phalloidin was rotated to the direction of flow. Automated quantification by the ImageJ plugin OrientationJ[83,84] evaluated the orientation of actin filaments using a Gaussian function of standard deviation with a Cubic Spline gradient to produce an event distribution of all local angles relative to flow. The distribution of orientation as a frequency of events at 30 degree intervals was determined. The OrientationJ plugin was also used to generate a visual of the local directional analysis using the same Gaussian window σ and Cubic Spline gradient.

Western blotting analysis

Western blotting was made as described by us.[82] For knock down experiments, cell lysates were collected using Radioimmunoprecipitation assay (RIPA) buffer (Thermo Fisher, Cat # R027). For determination of AKT and ERK phosphorylation, cell lysates were washed 2 times with cold PBS and collected using lysis buffer (20 mM HEPES-KOH, pH 7.8, 50 mM KCl, 1 mM EGTA, 1% NP40, 1 mM NaF, 1 mM Na_3VO_4). Total protein concentrations were measured using a Bicinchoninic acid (BCA) protein assay kit (Thermo Scientific; cat# 23225). Samples were boiled in Laemmli sample buffer (Bio-Rad; cat# 1610747) for 10 min and separated using a SDS-PAGE system. Proteins were transferred to nitrocellulose membranes overnight at 4°C. Membranes were blocked in 5% BSA for 1–2 hours. Proteins of interest were then detected by probing with the indicated primary and horseradish peroxidase–conjugated secondary antibodies. In the experiments where greater protein separation was needed, for example, for Piezo1 detection, vinculin and α-tubulin were used as loading controls because of their higher molecular weight. In the experiments detacting AKT and ERK phosphorylation, GAPDH was used as loading control due to variability in β-actin protein expression under flow conditions. Following incubation with secondary antibodies, proteins were detected using chemiluminescence and Premium Autoradiography film (lab Force, cat# 1141J52). Band intensities were quantified using densitometry analysis using ImageJ software (National Institute of Health).

Curve fit and quantification of rate constants

GraphPad Prism9 software was used to fit a linear regression to the ER Ca^{2+} rise and one phase exponential decay regression to fit ER Ca^{2+} decay. To calculate the rate constant for ER Ca^{2+} rise, a linear regression defined as y = yIntercept + Slope*x was used. To calculate the rate constant of ER Ca^{2+} decay, a one phase exponential decay regression defined as y= (y0 - Plateau)*exp(-K*x) + Plateau, where K is the rate constant for ER Ca^{2+} decay was used.

Vasodilation measurement in mouse mesenteric arteries

Mesenteric arteries from EC-restricted Piezo1 knockout mice and wild type C57BL/6 mice were used to measure flow-induced vasodilation as described previously.[85] Briefly, mice were euthanized by CO2 inhalation followed by cervical dislocation. Mesenteries were extracted and removed of all fatty tissues to isolate arterioles. Arterioles were divided into two pieces and incubated with adenoviral particles carrying the empty vector or encoding myr-Akt1 for 48 hours at 37 °C, 5% CO_2. First order arteries (120–180 μm in diameter) were cannulated into a flow-chamber, and rested for 30 minutes under 60 cm H_2O internal pressure (resting diameter). Endothelin-1 (120 pM) was applied to pre-constrict the vessel to respond to flow (pre-constrict diameter). Internal flow was generated by a pressure gradient between two reservoirs connected to each end of the cannulated vessel at Δ10, Δ20, Δ40, Δ60, and Δ100 cm H_2O, while the internal pressure was maintained at 60 cm H_2O. Flow-induced vasodilation was measured after 3 minutes of each pressure gradient applied (flow-induced diameter). Papaverine (100 μM), an endothelial independent vasodilator, was applied after vasodilation measurement at Δ100 cm H_2O to confirm smooth muscle functionality in vasodilation. Data were calculated using following equation:

Vasodilation (%) = (flow-induced diameter – pre-constrict diameter)/(resting diameter – pre-constrict diameter)*100.

QUANTIFICATION AND STATISTICAL ANALYSIS

Statistical significance was calculated using GraphPad Prism9 software (GraphPad). Student's *t*-test was used for experiments with two experimental groups. One-way ANOVA with Tukey's test was used for experiments with two or more experimental groups. For flow-induced vasodilation experiments statistical analysis was performed using two-way ANOVA, and the data were presented as mean ± standard error.